# Phase Diagram and Photopolymerization Behavior of Mixtures of UV-Curable Multifunctional Monomer and Low Molar Mass Nematic Liquid Crystal

**Domasius Nwabunma,[†] Kap Jin Kim,[†,‡] Yuhui Lin,[§] L. C. Chien,[§] and Thein Kyu*[,†]**

*Institute of Polymer Engineering, The University of Akron, Akron, Ohio 44325, and Liquid Crystal Institute, Kent State University, Kent, Ohio 44242*

*Received April 22, 1998; Revised Manuscript Received August 5, 1998*

ABSTRACT: A miscibility phase diagram of mixtures of UV-curable multifunctional thiolene-based optical adhesive (NOA65) and low molar mass 4-*n*-heptyl-4-cyanobiphenyl nematic liquid crystal (K21) has been established using light scattering, optical microscopy, and differential scanning calorimetry. The emergence of phase morphology was investigated during the heating and cooling cycles to identify various coexistence regions. A teapot phase diagram was obtained in which an upper critical solution temperature (UCST) overlapped with the nematic−isotropic transition of the liquid crystal. The phase diagram exhibited liquid + liquid, liquid + nematic, and pure nematic coexistence regions. Photopolymerization was carried out on various mixtures of NOA65 and K21 to fabricate polymer/liquid crystal composites by initiation in the one-phase and two-phase regions of the phase diagram. The rate constants for propagation and termination reactions ($k_p$ and $k_t$) were determined as functions of temperature and conversion. On the basis of the observed $k_p$ and $k_t$, the conversion rate was calculated by solving the rate equations for the photopolymerization process. It was found that the maximum conversion rate increased with increasing temperature and initial monomer concentration. The experimental results were in good accord with the calculated results in terms of both the order of magnitude and the trend. Of particular interest was that the domain morphology was uniformly distributed for the curing in the single phase, whereas the curing in the two-phase region resulted in nonuniformity of domain sizes.

## Introduction

Photopolymerization has been central to fabrication of polymer/liquid crystal composite films with desired structures and physical properties.[1−7] Photopolymerization entails the use of radiation such as ultraviolet (UV) or tunable laser light sources to polymerize and cross-link multifunctional photoreactive monomers. The technique is of immense interest scientifically and technologically because of its several advantages over thermal curing. The major advantages of photopolymerization are fast curing speed, uniformity, and ease of controlling the reaction. Polymerization temperature can be low; therefore, the loss of volatile ingredients (e.g., monomer, curing agent, etc.) and degradation of polymer can be suppressed considerably. In addition, the photopolymerization process is solvent-free and clean, and thus it has diverse applications in the areas of polymer thin films, coatings, adhesives, composites, and advanced optical devices such as flat panel displays, optical switches, and photoimaging plates, among others.

In most formulations, two or more ingredients are involved in the polymerizing system. When one or both components are photopolymerized, the molecular weight of the polymerizing species increases, which in turn causes the system to be unstable, thereby inducing phase separation. It is well-known that the resulting phase-separated structures of such a polymerizing system can exert a profound influence on its physical properties. It is therefore of crucial importance to understand the emergence of two-phase structures during photopolymerization-induced phase separation (PIPS), which is ultimately determined by the competition between photopolymerization kinetics and the dynamics of reaction-induced phase separation.

Depending on the functionality of the starting monomer, linear, branched, or cross-linked network structures may emerge. The multifunctional (i.e., three or more functional sites) monomers are customarily sought for photopolymerization to achieve polymer networks with good mechanical strength and chemical and thermal stability. Several factors such as temperature, composition, and photoinitiator concentration can influence photopolymerization steps involving initiation, propagation, termination, chain transfer, and inhibition/retardation reactions. Other factors such as incident radiation intensity, sample thickness, and sample-to-radiation source distance may be kept constant to avoid further complications.

In this paper, we first establish the phase diagram of mixtures of multifunctional photoreactive thiolene-based optical adhesive (NOA65) and a single-component low molar mass nematic liquid crystal (K21) by means of light scattering, optical microscopy, and differential scanning calorimetry (DSC). The effects of temperature and monomer concentration on the photopolymerization behavior involving reaction rate constants, photopolymerization rates, and conversions are examined by using a photo-DSC method. On the basis of the experimentally determined rate constants, photopolymerization rates and conversions are computed theoretically for comparison with experimental results. The emergence of phase-separated structures and concomitant

* To whom correspondence should be addressed.
[†] The University of Akron.
[‡] Permanent address: Department of Textile Engineering, Kyung Hee University, 1 Seochun-ri, Kiheung-eup, Yongin-si, Kyunggi-do 449-701, Seoul, South Korea.
[§] Kent State University.

S0024-9297(98)00646-9 CCC: $15.00 
Published on Web 09/15/1998

nematic ordering during photopolymerization are examined in the one-phase and two-phase regions of the phase diagram. Of particular interest is the drastic difference between the domain morphologies emerging from the UV curing in the one- and two-phase regions of the phase diagram.

## Theoretical Scheme

Free-radical photopolymerization comprising initiation, propagation, and termination reactions may be described customarily by the following kinetic equations.[8,9]

$$\frac{d[R]}{dt} = \Phi I_a - k_i[R][M] \qquad [R]_{t=0} = 0 \tag{1}$$

$$\frac{d[P^\bullet]}{dt} = k_i[R][M] - k_t[P^\bullet]^2 \qquad [P^\bullet]_{t=0} = 0 \tag{2}$$

$$\frac{d[M]}{dt} = -k_i[R][M] - k_p[M][P^\bullet] \qquad [M]_{t=0} = [M]_0 \tag{3}$$

where [R] is the radical concentration of the photoinitiator, [P•] the total concentration of polymer radicals, and [M] the monomer concentration. The quantity $I_a$ is the absorbed radiation intensity in moles of photons (Einstein) per unit volume per second, $\Phi$ is the quantum yield (or photochemical efficiency), and $k_p$ and $k_t$ are the propagation and termination rate constants, respectively. Inherent in the above equations are the assumptions that $k_p$ is independent of polymer chain length and there are no chain transfer and/or inhibition reactions. For a thin film, $I_a$ is given by

$$I_a = \epsilon b I_0[C]_0 \exp(-\Phi\epsilon I_0 t) \tag{4}$$

where $I_0$ is the incident radiation intensity, $\epsilon$ is the absorption coefficient (molar absorptivity) of the photoinitiator at the wavelength of UV radiation employed, $[C]_0$ is the initial concentration of the photoinitiator, and $b$ is the sample thickness.

Equations 1−3 are a set of ordinary differential equations, which may be solved numerically for a photopolymerizing system with experimentally determinable parameters $\Phi$, $\epsilon$, $b$, $I_a$, $k_i$, $k_p$, $k_t$, and the initial concentrations. When the time dependences of [R], [M], and [P•] have been computed, the monomer fractional conversion, $\alpha$, and the rate of photopolymerization, $R_p$, may be determined respectively from the equations

$$\alpha = \frac{[M]_0 - [M]}{[M]_0} \qquad \alpha_{t=0} = 0 \tag{5}$$

$$R_p = k_p[M][P^\bullet] = k_p[M]_0(1-\alpha)[P^\bullet] \qquad (R_p)_{t=0} = 0 \tag{6}$$

Photopolymerization has been customarily analyzed based on the pseudo-steady-state kinetics.[8−12] This method assumes that all radical concentrations quickly reach the steady-state limit (i.e., $d[R]/dt$ and $d[P^\bullet]/dt$ are approximately zero). This assumption permits the determination of the pseudo-steady-state rate, $R_{pss}$, as follows:

$$R_{pss} = \frac{k_p}{k_t^{1/2}}(\Phi I_a)^{1/2}[M] \tag{7}$$

Equation 7 predicts the existence of an initial photopolymerization rate[11] given by

$$R_{pss(t=0)} = \frac{k_p}{k_t^{1/2}}(\Phi\epsilon b I_0[C]_0)^{1/2}[M]_0 \tag{8}$$

in which the initial rate varies linearly with the first power of the monomer concentration. Further, the rate varies linearly with the square root of the photoinitiator concentration and incident radiation intensity. It is worth mentioning that eq 7 is particularly useful in estimating experimentally the combined rate constant $k_p/(k_t)^{1/2}$ (see the Experimental Section).

On the other hand, the photopolymerization data from the isothermal photo-DSC runs show that the rate is zero at $t = 0$. Then, it quickly reaches a maximum value and thereafter decreases asymptotically to zero. It follows immediately that the pseudo-steady-state approximation would be inadequate to theoretically predict the experimental trend of the mixture of photoreactive monomer and liquid crystal. In such a situation, eqs 1−3 may be solved numerically.

## Experimental Section

**(i) Materials and Methods.** UV-curable thiolene-based optical adhesive liquid (NOA65) premixed with about 5 wt % benzophenone photoinitiator was purchased from Norland Products Inc., New Brunswick, NJ. NOA65 has a density of 1.12 g/cm$^3$, a molecular weight of 400 g/mol, and a maximum absorption in the 350−380 nm range.[14,16]

The single component 4-*n*-heptyl-4-cyanobiphenyl (K21, $T_{KI}$ = 28.5 °C and $T_{NI}$ = 42 °C) nematic liquid crystal was purchased from BDH Chemicals (a division of Merck), Poole, England. Both materials were used as received without further purification. K21/NOA65 mixtures of compositions 0/100, 50/50, and 95/05 by weight were prepared for photopolymerization by weighing appropriate amounts of K21 and NOA65 in vials and then thoroughly mixed without any solvent to achieve intimate mixing.

Prior to photopolymerization, the phase diagram of K21/NOA65 monomer mixtures was established experimentally by means of polarized optical microscopy, light scattering (cloud-point measurement), and DSC. The theoretical phase diagram was calculated following the method of Shen and Kyu.[17] In this paper, only the experimental procedure is presented, and interested readers are referred to the original paper of Shen and Kyu[17] for the detailed theoretical procedure.

For the optical microscopy experiment, a Nikon Optipot 2-POL microscope with a 12 V, 100 W, filtered halogen light source was used. The magnification was 400×. Pictures were taken using photographic attachments composed of a Nikon FX-35DX camera connected to a Nikon UFX-DX exposure controller. For sample heating and cooling, a sample heating stage (model TS1500, Linkam Scientific Instruments) interlinked with a Linkam programmable temperature controller (model TMS93) and a cooling system (Model LNP93/2) was utilized. Samples were placed under covered micro glass slides, then heated until they were optically clear, and cooled slowly to ambient temperature. Any phase transformation has been observed under the optical microscope during the heating/cooling cycles. The heating and cooling rates were 1 °C/min.

For the light scattering experiment, a 2 mW, randomly polarized He−Ne laser light source (Aerotech, model LSR2R) with a wavelength of 632.8 nm was used. Cloud points were measured by monitoring the scattered intensity at a fixed angle (∼10°) using a photodiode detector (Hamamatsu Co., model HC-220-01). A sample stage coupled with a programmable temperature controller (Omega, model CN-2012) with a resolution of ±0.1 °C was utilized for temperature scans at the rate of 1 °C/min. A personal computer was connected to

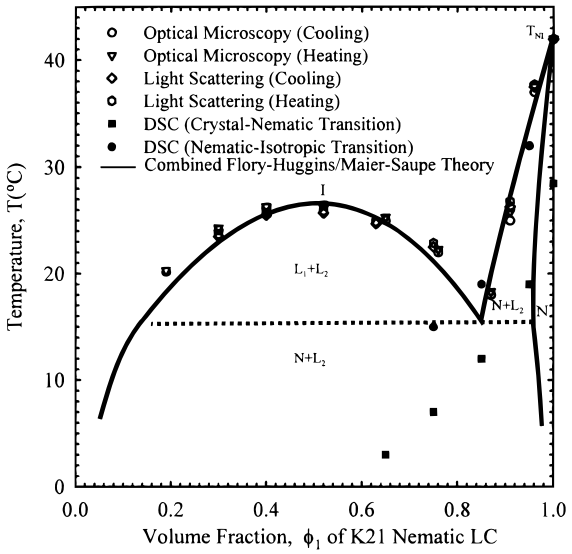


**Figure 1.** Phase diagram of the K21/NOA65 system obtained by means of light scattering, optical microscopy, and differential scanning calorimetry. Theoretical prediction (solid curve) based on the combined Flory−Huggins (F−H) and Maier−Saupe (M−S) theories.[17]

the light scattering equipment via an A/D converter for data acquisition. The sample thickness was about 10−20 $\mu$m.

DSC experiments were performed by means of a Du Pont thermal analyzer (model 9900) equipped with a DSC module and interfaced with an IBM-compatible computer for data acquisition and analysis. Liquid nitrogen was used for cooling. Temperature scans were conducted at a heating rate of 5 °C/min from −25 to +50 °C. Samples, weighing about 10−15 mg, were placed in sealed hermetic pans and purged with nitrogen gas.

**(ii) Photopolymerization.** Photopolymerization was carried out isothermally at two temperatures (20 and 40 °C) corresponding to two-phase and a one-phase regions of the phase diagram of the LC/NOA65 mixture (see Figure 1). Prior to photopolymerization, the mixture was heated to the isotropic region to ensure homogeneity and uniformity of the film. It was then brought back to the intended experimental temperatures for photopolymerization. Photopolymerization reactions were monitored using a Perkin-Elmer DSC instrument equipped with a dual-beam photocalorimetric accessory (DSC-DPA7). The photocalorimetric accessory included a monochromator to select UV radiation of a specific wavelength (366 nm) from a xenon light source (450 W). Each mixture was weighed (5−15 mg) and placed in a hermetic aluminum DSC pan. Prior to the application of the UV radiation, the DSC cell was flushed with nitrogen for about 5 min to prevent oxidation. During photopolymerization, the sample and the reference pans were left uncovered in the photo-DSC.

Prior to theoretical calculations, the $k_p$ and $k_t$ of NOA65 monomers were first experimentally determined as functions of temperature and conversion. NOA65 was premixed with benzophenone photoinitiator.[14] Benzophenone photoinitiator underwent photodecomposition in the presence of a tertiary amine activator to yield two different radicals, with only one of the radicals initiating the photopolymerization.[13] NOA65 presumably contains a tertiary amine.[14] Benzophenone molar absorptivity, $\epsilon$, at a wavelength of 366 nm was reported[15] to be 85 mol$^{-1}$ L cm$^{-1}$. The quantum efficiency $\Phi$ was assumed to be unity. All other parameters used in our calculations may be determined experimentally. Equations 1−3 may then be solved numerically based on the fourth-order Runge−Kutta method. The calculated results have been discussed by comparison with the experimental data.

**(iii) Estimation of Photopolymerization Rate and Conversion.** The heat flow versus time data from the isothermal photo-DSC were used to calculate the experimental conversion rate (s$^{-1}$) and the photopolymerization rate (mol L$^{-1}$ s$^{-1}$) based on the equations[18]

$$\frac{d\alpha}{dt} = \left(\frac{dH}{dt}\right)\frac{1}{\Delta H^\circ m} \tag{9}$$

$$R_p = \left(\frac{d\alpha}{dt}\right)[M]_0 \tag{10}$$

where $dH/dt$ (J s$^{-1}$) is the differential heat flow, $\Delta H^\circ$ (J g$^{-1}$) the heat of polymerization for 100% conversion of NOA65, $[M]_0$ (mol L$^{-1}$) the initial concentration, and $m$ (g) the mass of NOA65 in the mixture. Note that eq 9 ignores the heat produced during initiation and termination, if any.

Assuming that the heat evolved during polymerization is proportional to the amount of NOA65 reacted, the fractional conversion may be calculated as follows:

$$\alpha = \frac{\Delta H^t}{\Delta H^\circ m} \tag{11}$$

where $\Delta H^t$ (J) is the apparent heat of polymerization for incomplete NOA65 conversion obtained from the numerical integration of the area under the digitized heat flow curve up to time $t$; i.e., $\Delta H^t = \int_0^t (dH/dt)\, dt$. For NOA65, $\Delta H^\circ$ for the full conversion was estimated from the data of Smith.[16] Using the estimated values of $\Delta H^\circ$ (9.52 J/g at 20 °C and 11.90 J/g at 40 °C),[16] the conversions for the photopolymerized mixtures were then calculated. Since $\alpha$ is known experimentally, the concentration of the unconverted NOA65 monomer may be calculated by the following equation:

$$[M] = (1 - \alpha)[M]_0 \tag{12}$$

**(iv) Estimation of Propagation and Termination Rate Constants.** The rate constants $k_p$ and $k_t$ as functions of temperature and conversion may be estimated from the data of two separate experiments: (i) photopolymerization under constant illumination (i.e., pseudosteady state) and (ii) photopolymerization under intermittent illumination (often known as an unsteady-state "dark" reaction).

First, the combined rate constant, $k_p/(k_t)^{1/2}$, may be determined as a function of conversion at each temperature from eq 7 based on the pseudosteady state as follows:

$$\frac{k_p}{k_t^{1/2}} = \frac{R_{pss}}{(\Phi I_a)^{1/2}[M]} \tag{13}$$

where $R_{pss}$ and $[M]$ are known experimentally. The absorbed intensity, $I_a$, may be calculated according to eq 4. The combined rate constant $k_t/k_p$ may be estimated from the slope of the $[M]/R_p$ versus $t - t_c$ plot for various conversions, $\alpha_{t_c}$, according to the equation

$$\frac{[M]}{R_p} = \frac{k_t}{k_p}(t - t_c) + \frac{[M]_{t_c}}{(R_p)_{t_c}} \tag{14}$$

where $t_c$ is the time at which UV irradiation was stopped for the "dark" reaction to take place. When $k_p/(k_t)^{1/2}$ and $k_t/k_p$ are known, the individual rate constants $k_p$ and $k_t$ may then be obtained.

## Results and Discussion

**(i) Phase Diagram.** Prior to photopolymerization, a temperature−composition phase diagram of the K21/NOA65 monomer mixture was first established to determine the thermodynamic stability and to identify various coexistence regions. Figure 1 depicts the phase diagram obtained from light scattering, optical microscopy, and DSC experiments. The solid line represents the theoretical coexistence curve calculated self-consistently according to the combined Flory−Huggins

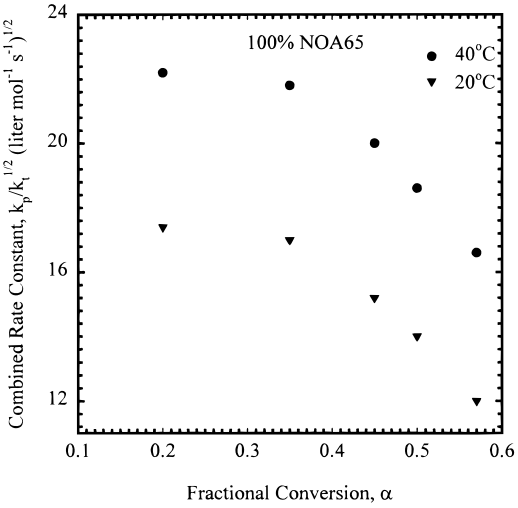


**Figure 2.** Combined rate constant, $k_p/(k_t)^{1/2}$, versus fractional conversion, α, for 20 and 40 °C photopolymerization. Data were obtained based on the pseudo-steady-state (constant illumination) kinetic analysis.

theory for isotropic mixing and the Maier−Saupe theory for nematic ordering.[17] The phase diagram reveals pure nematic, liquid + liquid, and liquid + nematic coexistence regions. The 50/50 mixture is isotropic at 40 °C but is in the two-phase liquid−liquid ($L_1 + L_2$) region at 20 °C. On the other hand, the 95/05 mixture is isotropic at 40 °C but very close to the narrow nematic (N) region at 20 °C. The present phase diagram is consistent with the general phase diagrams reported for other mixtures of low molar mass nematic LC/flexible monomer (or flexible linear polymer).[17]

**(ii) Kinetic Behavior.** Figure 2 shows the plots of the combined rate constant $k_p/(k_t)^{1/2}$ versus conversion α at 20 and 40 °C. At both temperatures, $k_p/(k_t)^{1/2}$ decreases with α fairly slowly at low conversions but shows a strong decreasing trend at higher conversions. To separate $k_p$ and $k_t$, the reaction was allowed to proceed after turning off the UV light. Parts a and b of Figure 3 depict the plots of $[M]/R_p$ versus $t - t_c$ for various conversions, $\alpha_{t_c}$, at 20 and 40 °C, respectively. Note that $t_c$ represents the time at which the UV light was turned off and $\alpha_{t_c}$ the corresponding conversion. For each temperature, straight lines were obtained in the plots as predicted by eq 14. The ratio $k_t/k_p$ for each $\alpha_{t_c}$ was obtained from the slopes of the individual curves in Figure 3a,b. This $k_t/k_p$ ratio was further plotted against $\alpha_{t_c}$ in Figure 4. An approximate linear decrease in the ratio with $\alpha_{t_c}$ can be discerned as opposed to the nonlinear decrease in the ratio $k_p/(k_t)^{1/2}$ with $\alpha_{t_c}$ (Figure 2).

Figure 5 shows the rate constants, $k_p$ and $k_t$, as functions of conversion, α, at 20 and 40 °C, respectively. From the figure, a general decreasing trend is noticed in both cases, which is in good agreement with the behavior of the rate constants observed for various multifunctional monomers.[12,17,18] Another observation worth mentioning is that $k_p$ and $k_t$ are fairly constant at low conversions but decrease rapidly at higher conversions (Figure 5). The rapid decrease in $k_p$ at higher α may be a consequence of the shift from chemical-controlled to diffusion-controlled photopolymerization, while that of $k_t$ results from radical trapping and isolation during network formation. Another interesting observation is that $k_t$ appears to decrease more than $k_p$ with conversion at both temperatures, indicating that the termination reaction occurs more slowly than the propagation reaction.

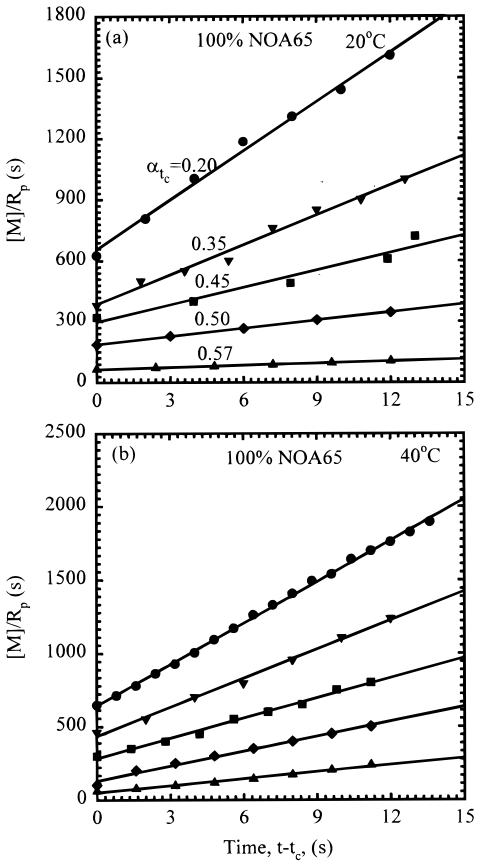


**Figure 3.** Plot of the ratio $[M]/R_p$ against $t - t_c$ for various fractional conversions, $\alpha_{t_c}$, at which the UV light shutter was closed. Data were obtained based on the unsteady-state (intermittent illumination) kinetic analysis at (a) 20 and (b) 40 °C.

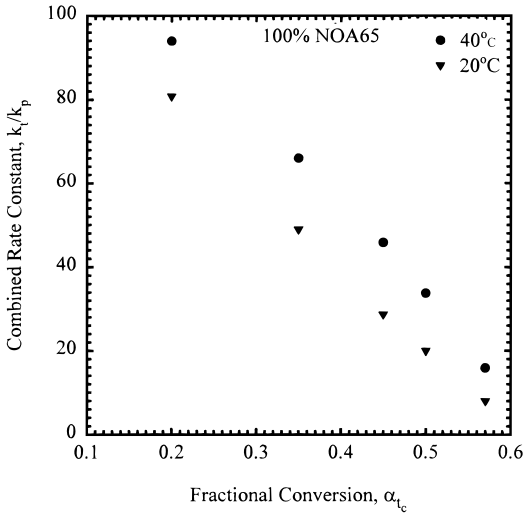


**Figure 4.** Combined rate constant $k_t/k_p$ versus fractional conversion, $\alpha_{t_c}$, at which the UV light shutter was closed. Data were obtained based on the unsteady-state (intermittent illumination) kinetic analysis at 20 and 40 °C.

Except for the fact the $k_p$ and $k_t$ values generally decrease with α, their exact relationship is not known. Although curve fitting of the rate constants versus conversion may be possible, $k_p$ and $k_t$ values at a given conversion were used at each temperature for simplicity. This simplification was done to evaluate the predictive

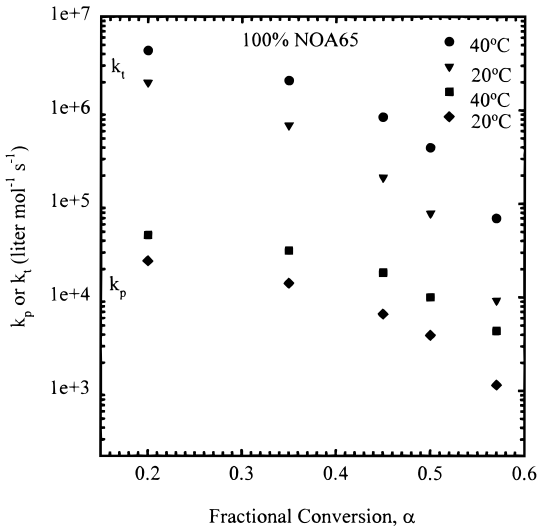


**Figure 5.** Rate constants $k_p$ and $k_t$ as functions of fractional conversion for NOA65 photopolymerization at 20 and 40 °C.

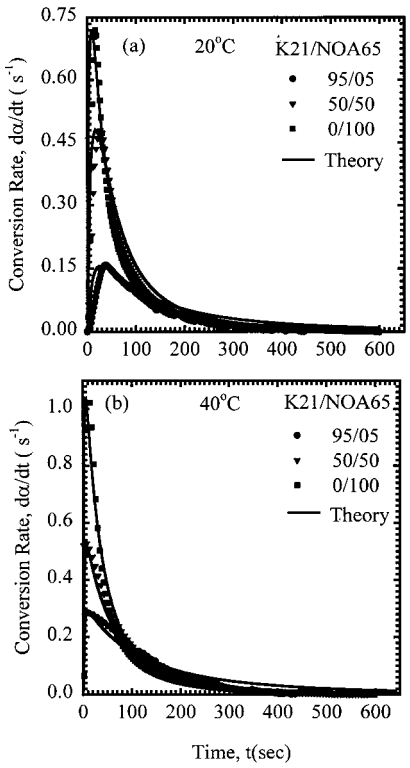


**Figure 6.** Experimental and theoretical (solid curves) conversion rates, d$\alpha$/d$t$, versus time $t$ for photopolymerization at (a) 20 and (b) 40 °C.

capability of the theory since curve fitting was not our primary goal.

**(iii) Photopolymerization Characteristics.** Parts a and b of Figure 6 show the experimental conversion rate, d$\alpha$/d$t$, as a function of time, $t$, at 20 and 40 °C in comparison with the theoretical curves. It is apparent that the conversion rate rises drastically at the onset of the reaction, quickly reaching the maximum rate, $(\mathrm{d}\alpha/\mathrm{d}t)_{max}$, within a few seconds. Subsequently, d$\alpha$/d$t$ decays asymptotically toward zero with time. The initial quick rise in the d$\alpha$/d$t$ versus $t$ plots may be attributed to the rapid generation of polymer radicals, reaching the maximum peak quickly in a manner dependent on the competition between the propagation and the onset of the termination reaction. The subsequent drop in the conversion rate may be ascribed to the effects of reduced polymer radical mobility, monomer depletion, and termination. As the concentration of monomer (NOA65) in the starting mixture increases, so does $(\mathrm{d}\alpha/\mathrm{d}t)_{max}$ at each temperature. This behavior is expected because LC molecules are not directly involved in the reaction. Furthermore, the $(\mathrm{d}\alpha/\mathrm{d}t)_{max}$ at 40 °C is greater relative to that at 20 °C for a given K21/NOA65 mixture. This may be attributed to an increase in the mobility of the polymerizing mixtures at the higher temperature.

Autoacceleration, associated with a continuous increase in the reaction rate with time (or with conversion), may occur during polymerization of certain neat monomers. This process is normally attributed to polymer radical trapping, causing $k_t$ to decrease faster than $k_p$ in a manner that causes $k_p/(k_t)^{1/2}$ to increase and, hence, $R_p$ to rise according to eq 7. However, our experimental result (Figure 2) for the LC/monomer mixture shows otherwise; i.e., the ratio $k_p/(k_t)^{1/2}$ decreases as both $k_t$ and $k_p$ decrease similarly with conversion (Figure 5). It is reasonable to infer that autoacceleration is highly unlikely to occur in this blend system. Although autoacceleration may have occurred during photopolymerization of the neat mesogenic monomers, we are unaware of any reported work that shows autoacceleration during photopolymerization of LC/monomer mixtures.

In the theoretical calculations, the $k_p$ and $k_t$ values at a given constant $\alpha$ (e.g., 0.2) were used instead of all the experimentally determined values to estimate the order of magnitude. Another reason is due to the lack of precision of the photo-DSC measurement in determining $k_p$ and $k_t$, particularly at high conversions. The theory is thus solely based on the chemically controlled propagation, in which the effect of diffusion-controlled propagation on the $k_p$ and $k_t$ values has been ignored. The observed $k_p$ and $k_t$ values used in the computations are those of the pure NOA65 and may not accurately apply to the mixtures. Despite these limitations of the theory, the calculated results capture the experimental trends at least qualitatively at both temperatures, except that the deviation in the results of curing at the two-phase region (20 °C) appears slightly larger than that in the one-phase region (40 °C).

Parts a and b of Figure 7 show the plots of experimental conversion rate, d$\alpha$/d$t$, against conversion, $\alpha$, at 20 and 40 °C, respectively, in comparison with the predicted theoretical curves. The $(\mathrm{d}\alpha/\mathrm{d}t)_{max}$ increases in magnitude within a few percent conversion irrespective of temperature and NOA65 concentration in the starting mixture, while the $(\mathrm{d}\alpha/\mathrm{d}t)_{max}$ peak positions are shifted slightly to a higher $\alpha$ with increasing NOA65 concentration. Although theoretically a full conversion is possible, experimentally it is difficult to achieve the complete conversion because of the diffusion-limited propagation, particularly in a multifunctional system, where the three-dimensional network is formed. Also, the limited sensitivity of the photo-DSC instrument in detecting heat evolved at later times and at high liquid crystal contents presents an additional factor. Nonetheless, the agreement between the experimental and calculated results in Figure 7 appears reasonably good.

**(iv) Emergence of Phase Morphology during Photopolymerization in the One- and Two-Phase Regions.** A major shortcoming which has been overlooked in the literature on photopolymerization of LC/monomer systems is that, in some cases, the starting

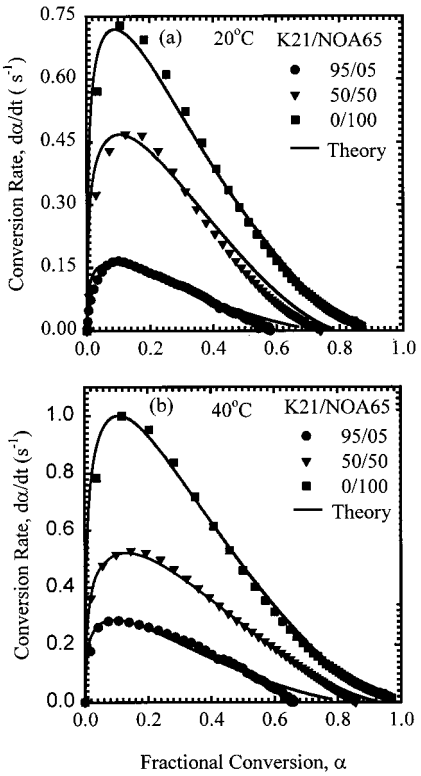


**Figure 7.** Experimental and theoretical (solid curves) conversion rates, d$\alpha$/d$t$, versus fractional conversion, $\alpha$, for photopolymerization at (a) 20 and (b) 40 °C.

mixtures have already phase-separated into two distinct phases prior to photopolymerization (e.g., 50/50 mixture at 20 °C in Figure 1). The initial concentrations of the starting NOA65 in the two phases are obviously different from one another. The rates of polymerization are, therefore, expected to be different for the LC-rich and monomer-rich phases. Even when the starting mixture is in the single phase (e.g., 50/50 and 95/05 NOA65/K21 mixtures at 40 °C in Figure 1), once reaction starts, the mixture will undergo phase separation due to the increase in molecular weight of the reacting monomer (NOA65).

Thus in both cases, a two-phase structure should emerge as depicted in the optical micrographs for the 95/05 K21/NOA65 mixture photopolymerized in the one-phase (40 °C) and two-phase (20 °C) regions of the phase diagram (Figure 8). However, it is apparent that the droplet morphology resulting from the curing in the single-phase region (40 °C) is more uniform relative to that from the curing in the two-phase region (20 °C). This may be due to phase separation occurring presumably via spinodal decomposition at 40 °C.[20] In fact, repeated photopolymerization starting in the single phase of the LC/monomer mixture always resulted in uniformly distributed phase-separated domains.

The above arguments support the claim that the emergence of domain morphology depends on thermodynamics (i.e., phase equilibrium of the starting mixtures) and kinetics of photopolymerization-induced phase separation. It is, therefore, of crucial importance to consider the coupling between the dynamics of phase separation and the reaction kinetics in future theoretical development. It is also known that both chemical reaction and phase separation are two antagonistic processes: the former triggering the latter by introducing thermodynamic instabilities to the blend system. It

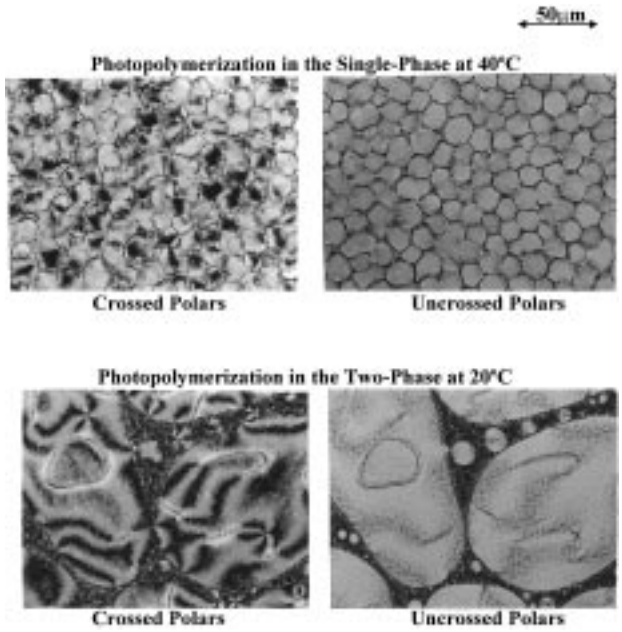


**Figure 8.** Morphology of the 95/5 K21/NOA65 mixture observed under crossed and uncrossed polarizers after photopolymerization in the one-phase (40 °C) and two-phase (20 °C) regions for 5 min.

is anticipated that the two processes may compete in a manner dependent on the thermodynamic state of the starting LC/monomer mixture, reaction conditions (time, temperature, UV intensity, etc.), and material constants ($T_{NI}$, $k_p$, $k_t$, etc.). In light of this, a theoretical study on the competing mechanisms has been undertaken and is left to the scope of a future work.[20]

**(v) Effect of Liquid Crystal Ordering on Photopolymerization Behavior.** With regard to the effect of nematic liquid crystal ordering on the experimental d$\alpha$/d$t$ versus time plots at both temperatures, the maximum conversion rate, $(d\alpha/dt)_{max}$, was found to decrease with increasing K21 liquid crystal content. This observation is consistent with the experimental results of others.[21−23] Perplies et al.[21,22] found a drastic decrease in the polymerization rate in the ordered nematic-rich phase during the photopolymerization of a series of mesogenic acrylates and methacrylates. Also, de Visser et al.[23] observed the reduction of the polymerization rates in the cholesteric state of cholesteryl acrylate. The systems studied by Perplies et al.[21,22] and de Visser[23] were neat LC monomers in contrast to ours, which is a mixture of low molar mass nematic LC and flexible monomer. The observed reduction in the photopolymerization rate in the neat LC has been attributed to the reduced molecular mobility within the liquid crystalline phase.[21−23] On the same token, it is plausible that the mutual diffusion of LC/NOA65 may be slowed due to the reduced mobility of the molecules in the LC entity.

However, the opposite behavior was reported for some mesomorphic systems in which polymerization rates were found to increase with decreasing temperature. The enhanced photopolymerization rate with increasing ordering of the mesophase has been observed during the photopolymerization of neat mesogenic monomers,[24−28] flexible monomer/ferroelectric LC mixtures,[19] and flexible monomer/smectic LC mixtures.[24] Such enhanced rates have been attributed to the segregation of the monomer within the smectic layers.[29] In the case of the

neat mesogenic monomers, the enhanced rates have been attributed to the autoacceleration, resulting in a large decrease in the termination rates relative to the propagation rates.[30,31]

Since opposing trends in the photopolymerization rates have been observed in liquid crystalline media, Hsu and Blumstein[32] cautioned that one should be very careful in transferring the photopolymerization characteristics of one mesomorphic system to another. To do so, one should ascertain that the starting mixture possesses the same mesophase structures if it is in the two-phase region[32] or the systems should be in a homogeneous state (single phase) prior to polymerization. Our results indicate exactly the same phenomena.

## Concluding Remarks

In this work, we have established the phase diagram of the mixtures of UV-curable multifunctional thiolene-based optical adhesive (NOA65) and low molar mass nematic liquid crystal solvent (K21). The phase diagram is essentially an UCST overlapping with the nematic−isotropic transition of the liquid crystal. We also demonstrated experimentally and theoretically the influence of temperature and monomer concentration on the photopolymerization behavior.

On the basis of the phase diagram, photopolymerization experiments were conducted starting in the one-phase (40 °C) and two-phase (20 °C) regions of the K21/NOA65 mixtures. Photopolymerization rate constants $k_p$ and $k_t$ were determined as functions of temperature and conversion from which the photopolymerization characteristics were calculated theoretically. The maximum conversion rate was found to increase with temperature and NOA65 concentration in the starting mixtures. The $(d\alpha/dt)_{max}$ peak positions shifted slightly to higher conversions with an increase in the NOA65 concentration. Experimentally it is difficult, if not impossible, to achieve 100% conversion because of the diffusion-limited propagation. The limited sensitivity of the photo-DSC instrument in detecting the evolved heat at later reaction times, particularly at high liquid crystal contents, is another factor that can influence the experimental results. Despite these deficiencies, the theory captures at least qualitatively the experimental trends except that the fit of the curing in the one-phase region is better than that in the two-phase region. Finally, it was shown that the domain textures of the photopolymerization initiated in the one-phase region were more regular and finer as compared to those cured in the two-phase region of the LC /monomer mixtures.

**Acknowledgment.** Support for this work by the NSF-STC Center for Advanced Liquid Crystal Optical Materials (ALCOM) via Grant 89-20147 is gratefully acknowledged.

## References and Notes

(1) Drzaic, P. S. *Liquid Crystal Dispersion*; World Scientific: Singapore, 1995.
(2) Doane, J. W. In *Liquid Crystals: Applications and Uses*; Bahadur, B., Ed.; World Scientific: Singapore, 1990; Chapter 14, p 361.
(3) Montgomery, G. P.; Smith, G. W.; Vaz, N. A. In *Liquid Crystalline and Mesomorphic Polymers*; Shibaev, V. O., Lam, L., Eds.; Springer: New York, 1994; Chapter 5, p 149.
(4) Chien, L.-C.; Boyden, W.; Citano, A. J. In *Liquid Crystalline Polymer Systems: Technological Advances*; Isayev, A. I., Kyu, T., Cheng, S. Z. D., Eds.; ACS Symposium Series 632; Americal Chemical Society: Washington, DC, 1996; Chapter 11, p 183.
(5) Percec, V.; Joasson, H.; Tomazos, D. In *Polymerization in Organized Media*; Paleos, C. M., Ed.; Gordon and Breach: Philadelphia, PA, 1992.
(6) Crawford, G. P.; Zumer, S. *Liquid Crystals in Complex Geometries Formed by Polymer and Porous Networks*; Taylor & Francis: London, U.K., 1996.
(7) Hoyle, C. E.; Griffin, A. C.; Kang, D.; Chawla, C. P. In *Irradiation of Polymeric Materials*; Reichmanis, E., O'Donnell, J. H., Frank, C. W., Eds.; American Chemical Society: Washington, DC, 1993; Vol. 527, p 118.
(8) Odian, G. *Principles of Polymerization*; McGraw-Hill Book Company: New York, 1991.
(9) Billmeyer, F. W. *Textbook of Polymer Science*; John Wiley & Sons: New York, 1984.
(10) Moore, J. E.; Schroeter, S. H.; Shultz, A. R.; Stang, L. D. *ACS Symp. Ser.* **1976**, *25*, 90.
(11) Joshi, M. G. *J. Appl. Polym. Sci.* **1981**, *26*, 3045.
(12) Tryson, G. R.; Shultz, A. R. *J. Polym. Sci., Polym. Phys. Ed.* **1979**, *17*, 2059.
(13) Decker, C. In *Radiation Curing in Polymer Science and Technology*; Fouassier, J. P., Rabek, J. F., Eds.; Elsevier Applied Science: London, 1993; Vol. III, Chapter 2, p 53.
(14) Technical Data Sheet for NOA65 Optical Adhesive, Norland Products, Inc., New Brunswick, NJ.
(15) Fouassier, J. P. In *Radiation Curing in Polymer Science and Technology*; Fouassier, J. P., Rabek, J. F., Eds.; Elsevier Applied Science: London, 1993; Vol. I, Chapter 2, p 54.
(16) Smith, G. W. *Mol. Cryst. Liq. Cryst.* **1991**, *196*, 89.
(17) Shen, C.; Kyu, T. *J. Chem. Phys.* **1995**, *102*, 556.
(18) Cook, W. D. J. *Polym. Sci., Part A: Polym. Chem.* **1993**, *31*, 1053.
(19) Guymon, C. A.; Bowman, C. N. *Macromolecules* **1997**, *30*, 1594.
(20) Nwabunma, D.; Chiu, H.-W.; Kyu, T., in preparation.
(21) Perplies, E.; Ringsdorf, H.; Wendorff, J. H. *Makromol. Chem.* **1974**, *175*, 553.
(22) Perplies, E.; Ringsdorf, H.; Wendorff, J. H. *J. Polym. Sci., Polym. Lett. Ed.* **1975**, *13*, 243.
(23) de Visser, A. C.; de Groot, H.; Feyen, J.; Bantjes, A. *J. Polym. Sci., Polym. Chem. Ed.* **1971**, *9* 1893.
(24) Broer, D. J.; Mol, G. N. *Makromol. Chem.* **1989**, *190*, 19.
(25) Hoyle, C. E.; Kang, D.; Jariwala, C.; Griffin, A. C. *Polymer* **1993**, *34*, 3070. Hoyle, C. E.; Kang, D.; Chawla, C. P.; Griffin, A. C. *Polym. Eng. Sci.* **1992**, *32*, 1490.
(26) Hoyle, C. E.; Watanabe, J.; Whitehead, J. B. *Macromolecules* **1994**, *27*, 6581.
(27) Broer, D. J.; Boven, J.; Mol, G. N.; Challa, G. *Makrolmol. Chem.* **1989**, *190*, 2255.
(28) Broer, D. J.; Hikmet, R. A. M.; Challa, G. *Makromol. Chem.* **1989**, *190*, 3201.
(29) Guymon, C. A.; Bowman, C. N. *Macromolecules* **1997**, *30*, 9271.
(30) Hoyle, C. E.; Chawla, C. P.; Kang, D.; Griffin, A. C. *Macromolecules* **1993**, *26*, 758.
(31) Hoyle, C. E.; Watanabe, T. *Macromolecules* **1994**, *27*, 3790.
(32) Hsu, E. C.; Blumstein, A. *J. Polym. Sci., Polym. Lett. Ed.* **1977**, *15*, 129.

MA9806460